

Flux-tunable transmon incorporating a van der Waals superconductor via an Al/AlO_x/4Hb-TaS₂ Josephson junction

Eliya Blumenthal,^{1, 2, *} Ilay Mangel,^{1, 2, *} Amit Kanigel,^{1, 2} and Shay Hacohen-Gourgy^{1, 2}

¹*Department of Physics, Technion – Israel Institute of Technology, Haifa 32000, Israel*

²*Helen Diller Quantum Center (Technion)*

Incorporating van der Waals (vdW) superconductors into Josephson elements extends circuit-QED beyond conventional Al/AlO_x/Al tunnel junctions and enables microwave probes of unconventional condensates and subgap excitations. In this work, we realize a flux-tunable transmon whose nonlinear inductive element is an Al/AlO_x/4Hb-TaS₂ Josephson junction. The tunnel barrier is formed by sequential deposition and full in-situ oxidation of ultrathin Al layers on an exfoliated 4Hb-TaS₂ flake, followed by deposition of a top Al electrode, yielding a robust, repeatable hybrid junction process compatible with standard transmon fabrication. Embedding the device in a three-dimensional copper cavity, we observe a SQUID-like flux-dependent spectrum that is quantitatively reproduced by a standard dressed transmon–cavity Hamiltonian, from which we extract parameters in the transmon regime. Across measured devices we obtain sub-microsecond energy relaxation (T_1 from 0.08 to 0.69 μ s), while Ramsey measurements indicate dephasing faster than our 16 ns time resolution. We also find a pronounced discrepancy between the Josephson energy inferred from spectroscopy and that expected from the Ambegaokar–Baratoff relation using room-temperature junction resistances, pointing to nontrivial junction physics in the hybrid Al/AlO_x/4Hb-TaS₂ system. Although we do not resolve material-specific subgap modes in the present geometry, this work establishes a practical route to integrating 4Hb-TaS₂ into coherent quantum circuits and provides a baseline for future edge-sensitive designs aimed at enhancing coupling to boundary and subgap degrees of freedom in vdW superconductors.

I. INTRODUCTION

Superconducting transmon qubits provide a mature circuit-QED (cQED) platform for coherent control and precision spectroscopy of mesoscopic superconducting phenomena [1]. In most implementations, the Josephson element is an Al/AlO_x/Al tunnel junction, which offers reliable fabrication and low loss but restricts the accessible superconducting order parameters and quasiparticle spectra to those of conventional *s*-wave aluminum.

Van der Waals (vdW) quantum materials offer an avenue to extend cQED to correlated and topological superconductors, where the order parameter, low-energy quasiparticles, and boundary modes can differ qualitatively from conventional tunnel junctions. Recent work has demonstrated compact transmon implementations leveraging vdW heterostructures, including crystalline parallel-plate capacitors and fully vdW Josephson elements using a flake transfer method [2, 3]. A practical requirement for bringing these materials into cQED is a repeatable junction process that forms a robust tunnel barrier on an exfoliated vdW surface and is compatible with standard transmon fabrication. As a concrete demonstration, we focus on the 4Hb polytype of TaS₂, which is a transition-metal dichalcogenide that forms a naturally occurring heterostructure of alternating 1T and 1H layers. It superconducts with $T_c \approx 2.7$ K and has been reported to exhibit signatures consistent with time-reversal symmetry breaking at T_c [4]. Scanning tunneling

spectroscopy has further reported zero-bias states at step edges and within vortex cores, consistent with boundary and subgap states in a topological nodal superconductor [5]. Recent phase-sensitive Little–Parks measurements in 4Hb-TaS₂ rings report π -shifted oscillations in a subset of devices, supporting non-*s*-wave pairing components [6]. At the same time, the low-energy gap structure remains under active discussion, including proposals of robust gapless superconductivity associated with multi-band pair breaking [7] and recent microwave cavity studies of phase stiffness in few-layer devices [8].

These developments motivate the integration of 4Hb-TaS₂ into coherent superconducting circuits. A transmon whose Josephson element interfaces Al and 4Hb-TaS₂ provides a controllable microwave probe of the condensate and of potential subgap degrees of freedom, complementary to tunneling microscopy and transport. Here we take a first step toward this goal by realizing a flux-tunable transmon in which the Josephson element is an Al/AlO_x/4Hb-TaS₂ junction. We demonstrate standard spectroscopy and time-domain control in a 3D cQED architecture, establishing an experimental baseline and a fabrication route for future edge-sensitive device geometries.

II. DEVICE DESIGN AND FABRICATION

Devices were fabricated on Si/SiO₂ substrates (250 μ m Si, 285 nm thermal oxide) pre-patterned with an alignment grid of either Pt/Cr (20 nm/5 nm) or Nb (25 nm). Substrates were solvent-cleaned by sequential sonication (5 min each in acetone, ethanol, and IPA) and baked at

* These authors contributed equally to this work.

180 °C for 2 min.

Flakes of 4Hb-TaS₂ were exfoliated via a dry-transfer method onto the prepared substrates. Candidate flakes were identified by optical microscopy and registered to nearby alignment markers. The substrate was coated with a PMMA trilayer resist stack (two layers of 495 A4 followed by 950 A2), and patterned using electron-beam lithography (RAITH e-Line 150, 10 kV). It was then developed in 1:3 MIBK:IPA (90 s), and rinsed in IPA. A short oxygen-plasma ashing step (30 s) was used to reduce resist residues in exposed areas.

Metal deposition was performed in an e-beam evaporator using a multi-step process designed to form a controlled tunnel barrier on exfoliated vdW crystals. First, an in-situ Ar ion mill removed surface contamination and milled a few nanometers into the 4Hb-TaS₂ at ~45° incidence to promote robust side-contact at junction interfaces. A short Ti gettering evaporation was used to reach base pressure. A nominal ~1 nm AlO_x barrier was produced by sequential deposition of 2–3 thin Al layers at 10° tilt (~5 Å each at ~0.5 Å/s), each fully oxidized in situ (80 Torr, 5% O₂ in Ar, 40 min) before the next deposition. A top Al layer (~200 nm) was then deposited at the same tilt angle. Lift-off was performed in NMP at 80 °C for 3 h, followed by IPA rinse and N₂ dry.

We implemented two SQUID-based transmon layouts (Fig. 1). In *Design 1*, the SQUID loop is placed between one capacitor pad and the 4Hb-TaS₂ flake, while the second pad connects to the opposite side of the flake via a larger contact. In *Design 2*, an asymmetric SQUID geometry was used to reduce sensitivity to supercurrent pathways through the flake bulk: one branch contains hybrid Al/AlO_x/4Hb-TaS₂ junction element(s), while the other branch contains a conventional Al/AlO_x/Al junction element. We fabricated and cooled down 2 samples of Design 1 and 3 samples of Design 2.

Individual devices were cleaved and mounted in a 3D OFHC copper cavity. The cavity–qubit assembly was cooled to a base temperature of ~10 mK in a dilution refrigerator. Standard filtered and attenuated microwave lines provided cavity readout and qubit control. A superconducting coil mounted above the cavity applied a DC magnetic field threading the SQUID loop to tune the effective Josephson energy.

III. RESULTS

A. Two-tone spectroscopy and parameter extraction

We performed two-tone spectroscopy by driving the cavity near its fundamental mode while sweeping a second tone to probe transmon transitions. Figure 2 shows a representative flux-dependent spectrum. The observed transitions are accurately captured by a standard

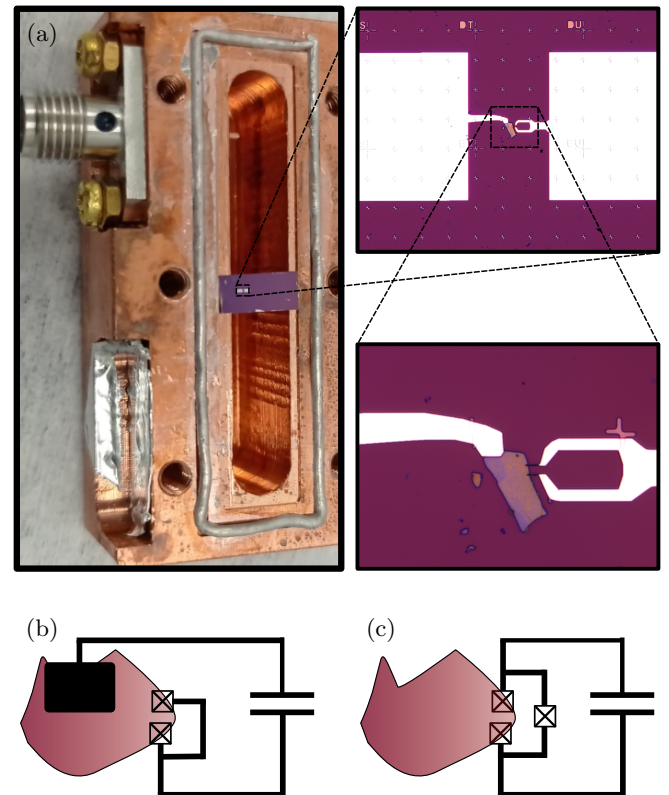


FIG. 1. (a) Photograph of the 3D copper cavity package and optical micrographs of a device 1B. (b,c) Schematic layouts of SQUID-transmon design 1 and 2. Design 1 routes supercurrent through the flake between the capacitor pads; Design 2 uses an asymmetric SQUID to reduce sensitivity to bulk transport through the flake.

transmon–cavity Hamiltonian,

$$\hat{H} = \hbar\omega_c \hat{a}^\dagger \hat{a} + 4E_C \hat{n}^2 - E_J(\Phi) \cos \hat{\phi} + \hbar g(\hat{a}^\dagger + \hat{a}) \hat{n}, \quad (1)$$

where ω_c is the cavity frequency, E_C the charging energy, $E_J(\Phi)$ the flux-dependent Josephson energy of the SQUID, \hat{n} and $\hat{\phi}$ are conjugate charge and phase operators, and g is the capacitive coupling rate. For a SQUID, the Josephson energy is

$$E_J(\Phi) = E_{J,\Sigma} \cos(\pi\Phi/\Phi_0) \sqrt{1 + d^2 \tan^2(\pi\Phi_0)}, \text{ where } E_{J,\Sigma} = E_{J1} + E_{J2}, d = (E_{J2} - E_{J1}) / (E_{J1} + E_{J2}) \text{ and } \Phi_0 \text{ is the magnetic flux quantum.}$$

For the device 1A in Fig. 2, we extract $E_C/h \approx 140$ MHz, $E_{J,\Sigma}/h \approx 11.6$ GHz and $d \approx 0.35$ corresponding to a maximum qubit frequency $\omega_{01}/2\pi \approx 3.46$ GHz and placing the device in the transmon regime ($E_J/E_C \gg 1$).

In addition to the primary transition, weaker lines appear at higher drive; these are consistent with multiphoton and cavity-assisted processes in the dressed transmon–cavity spectrum.

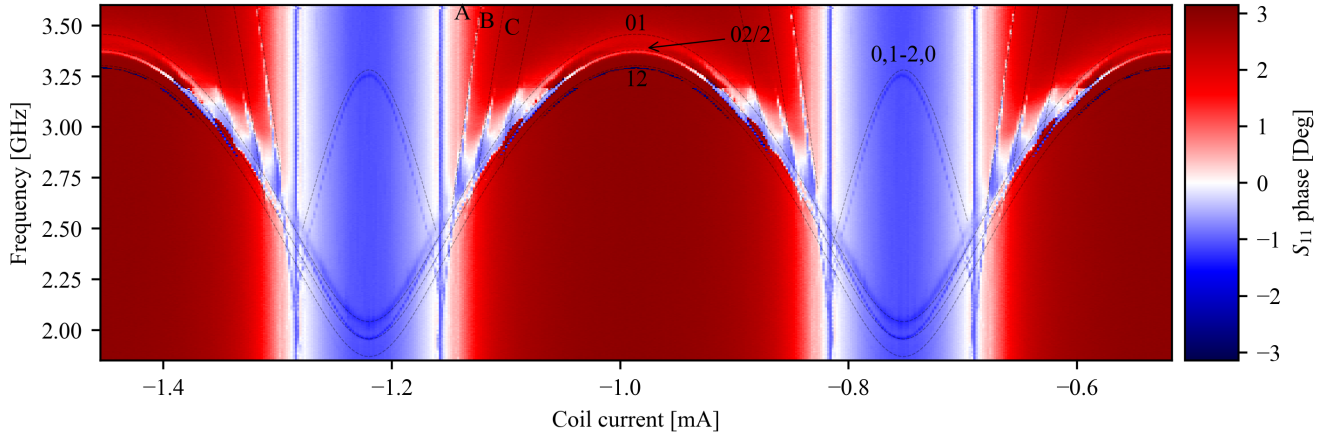


FIG. 2. Two-tone spectroscopy as a function of coil current (external flux). Dashed curves: transition frequencies obtained from diagonalizing the dressed Hamiltonian in Eq. 1 using extracted parameters. Weak additional features at high drive are consistent with cavity-assisted and multi-photon transitions within the dressed spectrum. The lines marked by A, B and C represent a Raman transition at a frequency of $(f_{1,0} - f_{0,0}) + (f_{3,0} - f_{0,1})$, $(f_{1,0} - f_{0,0}) + (f_{4,0} - f_{1,1})$ and $(f_{1,0} - f_{0,0}) + (f_{5,0} - f_{2,1})$, respectively. The 01 transition of the transmon is power-broadened.

Notably, the Ambegaokar–Baratoff relation [9]

$$E_J = \frac{\Phi_0 \Delta}{4R_n}, \quad (2)$$

with Δ the superconducting gap and R_n the junction's normal-state resistance, is not satisfied in our devices that use only Al/AlO_x/4Hb-TaS₂ junctions. For device 1B we extract a total Josephson energy of $E_{J,\Sigma}/h \approx 13.7$ GHz, while the junction resistances measured at room temperature are 2.4 kΩ (device 1A) and 1.9 kΩ (device 1B). Plugging these values into the relation yields an inferred gap of only 33–35 μV, which is inconsistent with the known gap of aluminum (~ 162 μV) [10] and the recently reported gap of 4Hb-TaS₂ (~ 390 μV) [11].

B. Time-domain coherence

We performed time-domain measurements on devices 1A and 2A. Energy relaxation was measured by applying a π -pulse followed by a variable delay and readout, yielding $T_1 = 0.08 \pm 0.01$ μs for device 1A and $T_1 = 0.69 \pm 0.03$ μs for device 2A (Fig. 3). Ramsey interferometry did not yield resolvable fringes. This indicates dephasing on a timescale shorter than our experimental time resolution of 16 ns, preventing a quantitative extraction of T_2^* with the present pulse sequence.

IV. DISCUSSION

The primary outcome of this work is the demonstration that an Al/AlO_x/4Hb-TaS₂ junction fabricated by a full-oxidation layer process functions as a coherent Josephson

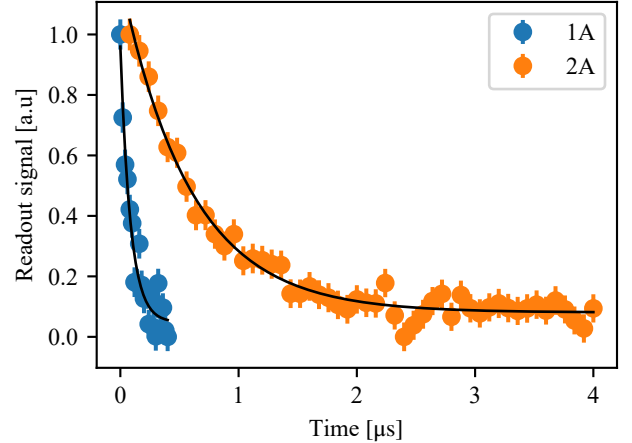


FIG. 3. Energy relaxation of devices 1A ($T_1 = 0.08 \pm 0.01$ μs) and 2A ($T_1 = 0.69 \pm 0.03$ μs).

element in a transmon, exhibiting a flux-tunable spectrum consistent with standard transmon physics and enabling time-domain control.

The Ambegaokar–Baratoff relation typically provides a reliable proxy for the Josephson energy in standard devices [12, 13]; interestingly, here there is a factor of ~ 5 discrepancy. Possible explanations for this discrepancy, arising from the unconventional superconductivity of 4Hb-TaS₂, include multigap structure in 4Hb-TaS₂ [11], anisotropic or sign-changing pairing that suppresses Josephson coupling [12], interface-dependent tunneling matrix elements that selectively couple to particular bands [13], and coupling to low-energy surfaces or edge modes in the 4Hb-TaS₂ [14, 15].

The observed relaxation times are below those of optimized $\text{Al}/\text{AlO}_x/\text{Al}$ transmons; however, this first-generation hybrid platform is primarily motivated by access to unconventional superconductivity rather than immediate lifetime benchmarking. In this context, it is important to identify plausible loss channels that are specific to the 4Hb-TaS₂ integration and that can guide future device optimization. Whether the high dephasing rate is a result of flux noise in the SQUID loops or is intrinsic to the 4Hb-TaS₂ requires further work. For example, an intrinsic mechanism might be quasiparticle-induced dephasing associated with enhanced subgap density of states in 4Hb-TaS₂, which could be exacerbated by a low effective gap energy.

A central motivation for this hybrid architecture is coupling to boundary and subgap degrees of freedom in 4Hb-TaS₂, including features reported in scanning tunneling spectroscopy at step edges and in vortex cores [5]. In the present geometry, several factors may suppress their visibility in transmon spectroscopy: supercurrent pathways dominated by bulk regions that shunt edge contributions; relevant mode energies outside the accessible measurement bandwidth; and junction separations and geometries that reduce coherent bound-state formation [16]. These considerations motivate future edge-sensitive junction layouts and higher-transparency weak links. Even without resolving such modes here, establishing coherent circuit operation is a prerequisite for applying the cQED toolbox as a spectroscopic probe of this material class. Finally, the many transitions observed at high drive power are well captured by the standard transmon–cavity model, underscoring that future searches for additional (“hidden”) transitions must account for the full coupled transmon–cavity Hamiltonian.

V. CONCLUSION

We demonstrated a flux-tunable 3D transmon qubit whose Josephson element is based on an $\text{Al}/\text{AlO}_x/4\text{Hb-TaS}_2$ junction fabricated via complete oxidation of a thin Al layer deposited onto an exfoliated 4Hb-TaS₂ flake and capped by Al. The device exhibits a well-behaved transmon spectrum with SQUID-like tunability and sub-

microsecond energy relaxation (T_1 in the 0.08–0.69 μs range across measured devices), while T_2^* could not be extracted from Ramsey measurements, as coherence decays on a timescale shorter than our 16 ns pulse-time resolution. This rapid dephasing may be related to quasiparticle dynamics in 4Hb-TaS₂: a comparatively low effective gap energy (e.g., from a small-gap band or enhanced subgap density of states) could support a higher nonequilibrium quasiparticle population and thereby increase quasiparticle-induced dephasing. Further work is required to determine whether T_2^* is limited intrinsically by the material or by extrinsic fabrication quality or flux noise. These results establish a practical route to integrating exfoliable vdW superconductors into coherent superconducting circuits, demonstrated here with 4Hb-TaS₂, and define a baseline for future circuit-QED studies that target boundary and subgap physics in this unconventional-superconductor platform.

For future work, we suggest etching the 4Hb-TaS₂ flake into a narrow strip for better control of the junction size and more defined edge mode coupling. Perhaps in this way a clear ABS might emerge. In addition, more work could be done to study the relation between the resistance and the Josephson energy of $\text{Al}/\text{AlO}_x/4\text{Hb-TaS}_2$ junctions.

VI. ACKNOWLEDGMENTS

We thank S. Frolov and V. Fatemi for helpful discussions. This research project was fully supported by the Helen Diller Quantum Center at the Technion.

VII. CONFLICT OF INTEREST

The authors declare no competing interests.

VIII. DATA AVAILABILITY

All data supporting the findings of this study are available upon reasonable request.

[1] J. Koch, T. M. Yu, J. Gambetta, A. A. Houck, D. I. Schuster, J. Majer, A. Blais, M. H. Devoret, S. M. Girvin, and R. J. Schoelkopf, Charge-insensitive qubit design derived from the cooper pair box, *Phys. Rev. A* **76**, 042319 (2007).

[2] A. Antony, M. V. Gustafsson, G. J. Ribeill, M. Ware, A. Rajendran, L. C. G. Govia, T. A. Ohki, T. Taniguchi, K. Watanabe, J. Hone, and K. C. Fong, Miniaturizing Transmon qubits using van der Waals materials, *Nano Letters* **21**, 10122 (2021).

[3] J. Balgley, J. Park, X. Chu, J. Liu, M. Holbrook, K. Watanabe, T. Taniguchi, A. Kamal, L. Ranzani, M. V. Gustafsson, J. Hone, and K. C. Fong, *Coherent and compact van der waals transmon qubits* (2025), arXiv:2512.08059 [quant-ph].

[4] A. Ribak, E. Lahoud, I. Silber, A. Almoalem, Y. Nagai, Y. Nakamura, E. N. Ribak, A. Kanigel, and H. Beidenkopf, Chiral superconductivity in the alternate stacking compound 4hb-tas₂, *Science Advances* **6**, eaax9480 (2020).

[5] A. K. Nayak, A. Steinbok, Y. Roet, J. Koo, G. Margalit, I. Feldman, A. Almoalem, A. Kanigel, G. A. Fiete, B. Yan, Y. Oreg, N. Avraham, and H. Beidenkopf, Evidence of topological boundary modes with topological nodal-point superconductivity, *Nature Physics* **17**, 1413 (2021).

[6] A. Almoalem, I. Feldman, I. Mangel, M. Shlafman, Y. E. Yaish, M. H. Fischer, M. Moshe, J. Ruhman, and A. Kanigel, The observation of π -shifts in the little-parks effect in 4hb-tas₂, *Nature Communications* **15**, 4623 (2024).

[7] D. Dentelski, E. Day-Roberts, T. Birol, R. M. Fernandes, and J. Ruhman, Robust gapless superconductivity in 4hb-tas₂, *Phys. Rev. B* **103**, 224522 (2021).

[8] T. Chistolini, H.-L. Kim, Q. Wang, S.-D. Chen, L. P. Cairns, R. P. Day, C. Sanborn, H. Kim, Z. Pedramrazi, R. Qi, T. Taniguchi, K. Watanabe, J. G. Analytis, D. I. Santiago, I. Siddiqi, and F. Wang, *Contactless cavity sensing of superfluid stiffness in atomically thin 4hb-tas₂* (2025), arXiv:2510.25124 [cond-mat.supr-con].

[9] V. Ambegaokar and A. Baratoff, Temperature dependence of the josephson current in superconducting tunneling, *Physical Review* **135**, A1069 (1964).

[10] M. A. Biondi and M. P. Garfunkel, Millimeter wave absorption in superconducting aluminum. i. temperature dependence of the energy gap, *Physical Review* **116**, 853 (1959), determines the superconducting gap in Al; reports $\Delta(0) = (3.2 \pm 0.1) k_B T_c$ with $T_c = 1.178$ K.

[11] H. Wang, Y. Jiao, F. Meng, X. Zhang, D. Dai, C. Tu, C. Zhao, L. Xin, S. Huang, H. Lei, and S. Li, *Evidence for multiband gapless superconductivity in the topological superconductor candidate 4hb-tas₂* (2024), arXiv:2412.08450 [cond-mat.supr-con].

[12] Y. Tanaka and S. Kashiwaya, Theory of josephson effects in anisotropic superconductors, *Physical Review B* **53**, 9371 (1996).

[13] A. Brinkman, A. A. Golubov, and M. Y. Kupriyanov, Multiband model for tunneling in mgb2 junctions, *Physical Review B* **65**, 180517 (2002).

[14] Y. Nagato, K. Nagai, and J. Hara, Theory of andreev bound states and tunneling spectroscopy in unconventional superconductors, *Journal of Low Temperature Physics* **103**, 1 (1996).

[15] M. Sato and Y. Ando, Topological superconductors: a review, *Reports on Progress in Physics* **80**, 076501 (2017).

[16] C. W. J. Beenakker, Universal limit of critical-current fluctuations in mesoscopic josephson junctions, *Phys. Rev. Lett.* **67**, 3836 (1991).